[SSC24-WI-03]

# Aerodynamic Satellite Attitude Control in Very Low Earth Orbit

Cheng Chang, Robert Breidenthal
Department of Aeronautics and Astronautics, University of Washington
Seattle, Washington, 98105; chang53@uw.edu
breident@uw.edu

Bo-Chuan Lin, Ya-Xun Yang
Department of Aeronautics and Astronautics, National Cheng Kung University
No.1-3, Daxue Rd., East Dist., Tainan city, 701, Taiwan(R.O.C); [+886 933290393]

## ABSTRACT

Simulation of a 3U-sized standard platform with four control panels attached to the rear part of the satellite at an altitude of 300 km was performed in Simulink to verify the feasibility of the aerodynamic control. The entire controller is composed of three loops: one outer loop and two inner loops. The outer loop is based on the robust and tested quaternion error feedback regulator to provide the target torque input for the two inner loops. The inner loops are responsible for actuating the control panels, using the square-root-based PI controller and a dedicated designed Panel Selecting Method (PSM) to achieve high-precision attitude control. The inner loop torque generation controller will determine when to switch to either a PSM or square-root PI controller based on the attitude error measured in the quaternion form. During the initial phase of the maneuver, the PSM will be in charge of pointing the satellite close to the desired attitude before the square-root PI controller takes over the control authority to achieve a smooth, steady-state response. The proposed aerodynamic control method will be compared with other controllers often used on the CubeSat platform, including the magnetorquer, to analyze the benefits of using aerodynamic control in various scenarios. Advantages like natural stabilization of the satellite's attitude in both pitch and yaw axes using almost zero electricity compared to magnetorquers will be discussed. However, the lifetime of a VLEO CubeSat is of concern at very low orbit where the atmosphere air density is relatively high, and the reduction of the lifetime on the given orbit from the increased drag of aerodynamic control surfaces will be addressed in the present work to discuss the impact of aerodynamic control on the operation of CubeSat at VLEO. With the results showing a reasonable detumbling time compared to the traditional magnetorquer at 300 km and a high degree of control accuracy with moderate variations of attitude near the level flight, the aerodynamic controller and the proposed algorithms are proven to be effective in the applications of near nadir pointing missions or missions requiring only the fast response of the rolling motion at VLEO environment. In the last section, some directions of future works will be shortly discussed, which include data-driven control for handling atmospheric conditions of other planets and the formation flight by using pure aerodynamic control.

## INTRODUCTION

The ever-increasing demand for the low earth observation mission for relevant applications in many industries through different remote sensing and imaging is driving the development of compact and affordable CubeSat operating at low altitudes for various benefits,[1] and the wide deployment of these small satellites at LEO will have a significant impact on increased collision hazard with other spacecrafts;[2] therefore, a simple actuator that can permit the CubeSat to work at lower altitude with controllable de-orbiting will largely address this issue while providing multiple advantages compared to satellites at regular Low-earth-orbit (LEO) altitude range from 600 to 2000 km.[3]

The very low earth orbit (VLEO), often referred to as the orbits below 450km,[3] features a dense atmosphere with a density several magnitudes higher than the traditional LEO environment. This environment reduces the lifetime of the satellite, so as space debris and uncontrollable spacecraft, ensuring space sustainability.[4] Besides, the remote sensing application also benefits from a lower orbit, because of the decreasing distance for imaging.[5] However,

the increased aerodynamic disturbances usually pose difficulties for traditional satellite attitude control, including the more severe reaction wheel saturation and the insufficient control authority provided by regular magnetic field-based actuators in comparison to the increased aerodynamic disturbance.[6]

Many previous studies have proposed both active and passive aerodynamic control methods to address the issues of traditional control strategies in harsh environments with strong aerodynamic disturbances.[2,3,7–9]

In the early research, passive-type aerodynamic control by using feathers or rotating control panels attached at the rear end of the satellites was mentioned to stabilize the spacecraft after the ejection away from the carrier.[7,9]

Active control methods to reduce the drag and precisely point the satellite to the desired attitude are therefore needed for practical applications, and several works of literature in[10] pointed out the feasibility of using feedback control design to actively adjust the control panels to realize the precise control.

A variety of control architectures implemented are based on the quaternion feedback controller as the outer loop for commanding the required torque to be actuated by control surfaces, with an inner loop for rotating the control panels accordingly .[3,7,9] The panel configuration algorithm (PCA) mentioned in[3,7] has a low settling time and overshoot with precise control of attitude in contrast to the traditional full-state feedback linear controller like the one presented in,[9] but the PCA has the feature of high-frequency rotation of control panels even when the desired attitude is achieved. This is caused by the nature that PCA only selects a finite number of possible panel configurations. Hence, it can't smoothly adjust the control surfaces like other full-state feedback controllers. Therefore, this paper aims to combine the advantages of both sides by incorporating the square-root proportion and integration (PI) controller and a PCA-based Panel Selecting Method (PSM) as the inner loop to realize the fast and precise actuation while removing the high-frequency vibration of the PCA method.

The atmosphere affects the satellite aerodynamic control performance undoubtedly. There are many atmospheric models available with the most frequently used one being NRLMSISE-00, which leverage measurement by satellite, rocket, and incoherent scatter radar, was featured in multiple research after 2000. Despite the air density of VLEO being far larger than LEO, the mean free path of the air molecules is still large compared to the continuous flow where the ratio of this two-length scale called Knudsen number (Kn) is smaller than 0.01.[11] When altitude is higher than 150km, for spacecraft smaller than 1 meter, the corresponding Kn is usually greater than 10. This situation is beyond the scope of either continuum or transition flows, and the aerodynamic effects are characterized by rarefied Gas-Surface Interaction (GSI).[12] To fully capture the influence of all gases and types of surfaces in the space on GSI, some past research even includes the computation of GSI for each gas, and the results are summarized in.[13]

Currently, for the simplification of analysis, most of the research adopted the Maxwell model for characterizing GSIs.[14] The GSI in this model can be categorized into two types, the diffusive and specular reflections, and the reasoned that the actual reflection in the rarefied gas flow should be the mixing of two types of reflections depending on the composition of local flow and the material of the surface at which flow incidences.[15]

To investigate aerodynamics control feasibility for satellites at cubesat scales in VLEO environments, this work is organized as follows. The aerodynamic control satellite design section includes the design and geometry of a 3U cubesat that will be tested in the simulation. The modeling section introduces the coordinate definitions, Euler's equation of motion, and the Quaternion kinematics. The aerodynamics effect analysis explains the atmospheric models used and the aerodynamic forces analysis. Then, the controller design section investigates the different control methods, including passive detumbling control, quaternion feedback regulator, panel selection method, square-root PI controller, and switch design. Simulation results verify that the control methods proposed in this work are feasible with acceptable performance for the high-precision and slow-motion pointing tracking capabilities. Finally, the conclusion summarizes this work and provides suggestions for future research with the data-driven controller.

## AERODYNAMIC CONTROL SATELLITE DESIGN

The aerodynamically-controlled 3U CubeSat studied in the present work is the modified model based on several previous works with "badminton" like control surfaces-body combination.[3,7] The satellite is composed of two parts: the central body and four control panels made of solar panels attached at the rear end of the main body. The rear-mounted control panels will guarantee the natural stabilizing

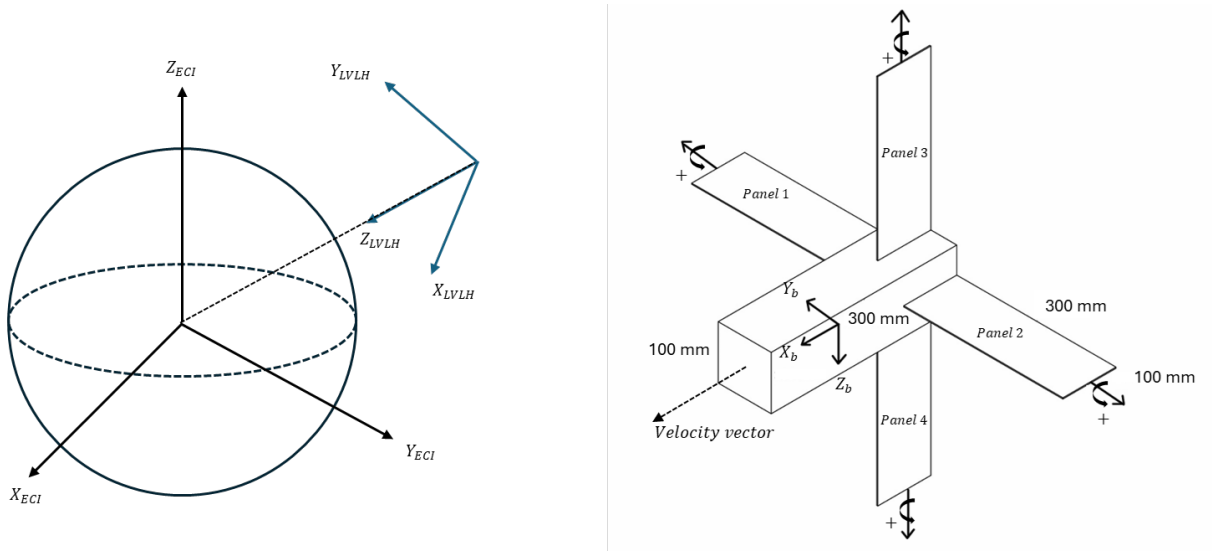


**Figure 1: The visual representation of frames used in the work (left) and the geometry design with the corresponding frame (right)**

effect to stabilize the satellite without any control effort. Control panels are also made long enough to avoid the blockade effect from the central body is small during moderate attitude maneuvers. The geometry of the satellite is shown in Figure. 1. Four control panels installed have different senses of rotation; control panels 2 and 3 are following the right-hand rotation convention while the panels 1 and 4 are opposite to it. Each of control panel can rotate around the rotational axis centered in the middle of the panels by a range of $\pm 90^0$ with the rotational rate saturated at 10 deg/sec and the response frequency of 10 Hz. The configuration of the 3U satellite and the corresponding definition for the coordinate system to be discussed in the next section is also presented as in Figure 1.

## MODELING

### *Coordinate Definitions*

This paper adopts three Cartesian reference coordinate systems: the Earth-centered inertial reference frame (ECI frame), Local Vertical, Local Horizontal (LVLH frame), and the body-fixed frame. The ECI frame has its center coincident with the center of mass of the earth, and three axes remain fixed to the distant stars and the chosen ECI coordinate for simulation is the J2K frame. The LVLH is defined in such a way that its positive Z-axis always points toward the center of the earth, and the Y-axis is parallel to the normal negative orbit while the X-axis coincides with the velocity vector of the spacecraft. The body-fixed frame has three axes fixed along the three principal axes of a typical symmetric spacecraft, and the center is at the location of the center of mass of the given spacecraft. The definition of frames can also be referred to the Figure 1.

### *Euler's equation of motion*

The rigid body rotation dynamic about the body-fixed axes with externally applied torque can be described with the following equation:

$$J\dot{\omega} = \Omega J\omega + u \tag{1}$$

where $\omega$ is the vector for the angular velocity measured in the body-fixed axes, $\Omega$ is a skew-symmetric matrix with three elements defined by the angular velocities, and J is the matrix of the momentum inertia. The matrix $\Omega$ is given as follows:

$$\begin{bmatrix} 0 & -\omega_3 & \omega_2 \\ \omega_3 & 0 & -\omega_1 \\ -\omega_2 & \omega_1 & 0 \end{bmatrix} \tag{2}$$

### *Quaternion Kinematics*

Although the Euler angle is commonly used in aviation, the four-element quaternion representation of attitude is chosen to avoid the singularities from occurring when the pitch angle is $\pm$ 90$^o$. Quaternion attitude representation can be related to the angular rates of body-fixed axes by the following equation:

$$\dot{q_v} = \frac{1}{2}\Omega q + \frac{1}{2}q_1\omega \tag{3}$$

$$\dot{q_1} = \frac{1}{2}\omega^T q \tag{4}$$

where $q_v$ is the vector part of the quaternion containing three elements of the quaternion vector., and $q_1$ is the scalar part with the scalar-last convention.

The outer loop controller, which uses the quaternion feedback to achieve the near eigenaxis rotation needs another measurement named quaternion error that is served as the major input for the controller. Quaternion error, which measures the error associated with the current and desired attitudes, is defined as follows:[16]

$$\begin{bmatrix} q_e \\ q_{2e} \\ q_{3e} \\ q_{4e} \end{bmatrix} = \begin{bmatrix} q_{4c} & q_{3c} & -q_{2c} & -q_{1c} \\ -q_{3c} & q_{4c} & q_{1c} & -q_{2c} \\ q_{2c} & -q_{1c} & q_{4c} & -q_{3c} \\ q_{1c} & q_{2c} & q_{3c} & q_{4c} \end{bmatrix} \begin{bmatrix} q_1 \\ q_2 \\ q_3 \\ q_4 \end{bmatrix} \tag{5}$$

where $q_c$ is the desired spacecraft orientation while $q_e$ is the calculated error between the current and the target attitudes.

## AERODYNAMICS EFFECT ANALYSIS

### *Atmospheric models*

To get an accurate satellite lifetime analysis, we leverage the widely used NRLMSISE-00 atmosphere model. This model is frequently used to predict satellite orbit decay and calculate atmosphere loss for satellite communication. This atmosphere model gives various air component densities, such as nitrogen, oxygen, helium, argon, and atomic oxygen. The total air density is included in the output. Also, the application height is across a wide range of altitudes, from sea level to 1000 km altitude, which is suitable for satellite lifetime calculation. This model is also build upon the data collected through past spacecraft and satellite missions.[17]

Although the NRLMSISE-00 is chosen for the long-period drag calculation and the lifetime analysis of the satellite for its high accuracy across a large range of altitude, the exponential model relates the density and altitude through the following equation:[18]

$$\rho = \rho_0 exp[-\frac{h - h_0}{H}] \tag{6}$$

is used for the real time simulation of control algorithms for its simplicity and computational efficiency. In this equation, h is the current altitude, $h_0$ is the reference altitude of 300 km, and H=50.828 Km is the scaled height while the nominal atmospheric density $\rho_0$ is 2.418e-11 $kg/m^3$.

### *Aerodynamic Drag and Torque Analysis*

For the rarefied GSI where the reflection of gas molecules on the incident surface are composed of specular and diffuse molecular reflection, the resulting normal force acting on the surface is governed by the molecular incident velocity and the material of the surface. The typical reported value of 0.8[7–9] for the accommodation coefficient is used in this paper, and this is the ratio of molecules reflected through the diffusion with a probability function of cosine. The surface roughness is critical to the control effectiveness of control surfaces, as reported in,[8] and the smoother the surface with lower accommodation coefficients, the more significant the improvement in the control performance.

The aerodynamic force exerted on the surfaces of the satellite and the corresponding drag and torque are mainly influenced by the relative free-stream velocity of incoming air to the satellite. The actual relative velocity of the air is the sum of the orbital velocity of satellite $v_{orbit}$, the varying atmospheric wind velocity $v_{wind}$, and the averaged velocity from the rotating atmosphere $v_{rot}$. To simplify the simulation without loosing the generality, the atmospheric wind isn't incorporated in the modeling.[3] The resulting relative wind velocity vectors, therefore, are found with the following expression:

$$v_{rel} = v_{orbit} + v_{rot} \tag{7}$$

By assuming the perfect circular orbit with an extremely small eccentricity, the orbital and the rotating atmospheric velocities can be calculated and related through the equations below:[8,19]

$$v_{rel} = \sqrt{\mu/R} \tag{8}$$

where $\mu$ is Earth's gravitational constant of $3.986 * 10^{14} \frac{m^3}{sec^2}$ and R is the orbit altitude plus the mean radius of earth $6.738 * 10^6 m$. The following relationship associates the angle $\beta$ with the orbital path and the local rotating atmosphere velocity:

$$\beta = \begin{cases} \pi - \arctan(\frac{d\lambda/dt}{d\phi/dt}), & \text{if } \frac{d\phi}{dt} < 0. \\ \frac{\pi}{2}, & \text{if } \frac{d\phi}{dt} = 0. \\ -\arctan(\frac{d\lambda/dt}{d\phi/dt}), & \text{if } \frac{d\phi}{dt} > 0 \end{cases} \tag{9}$$

where $\lambda$ and $\phi$ indicate the geodetic coordinates of latitude and longitude. Both $\lambda$ and $\phi$ can be propagated easily by using Simulink spacecraft dynamic block with the function of transferring the inertial frame coordinate to the geodetic coordinate. The resulting relative velocity vector can then be expressed

in the following way:

$$v_{rel} = R_{LVLH/Body} \begin{bmatrix} -||V_0|| + \omega_E||R||cos(\lambda)cos(\beta) \\ \omega_E||R||cos(\lambda)cos(\beta) \\ 0 \end{bmatrix} \tag{10}$$

where $R_{LVLH/Body}$ represents the direction cosine matrix (DCM) that rotates the LVLH frame to the body frame, $\omega_E$ is the Earth's rotation rate of $7.72 * 10^{-5}$ $rad/sec$, and R is the radius of the orbit from the center of earth.

With the resulting velocity vector, it's possible to find the torque exerted on the satellite by the aerodynamic forces on each surface. Only the reflection mechanism, including diffuse and specular reflection, is considered in this model. All generated torque will be enforced in the center of the geometry of the control surface. The resulting torque by summation of overall individual torques of all surfaces is found by the equation below with two coefficients $\sigma_t$ and $\sigma_n$ specifying the accommodation behavior of the GSI:

$$\begin{aligned} T = \rho||v_{rel}||^2 A_p[&\sigma_t(r_{m/p} * n_{rel}) \\ &+ (\sigma_t(v_b/||v_{rel}||) \\ &+ (2 - \sigma_n - \sigma_t)n_{rel} \cdot n_{normal})(r_{m/p} * n_{normal})] \end{aligned} \tag{11}$$

where $n_{rel}$ is the velocity unitary vector, $n_{normal}$ represents the surface normal vector, $r_{m/p}$ is the vector that connects the center of mass to the geometric center of the corresponding surface, and $\sigma_t$ and $\sigma_n$ is the tangential and normal momentum accommodation coefficient, $A_p$ is as follow:

$$A_p = H(n_{rel} \cdot n_{normal})n_{rel} \cdot n_{normal} A_{area} \tag{12}$$

where $A_{aera}$ is the surface area, H is the Heavyside step function that returns 1 when $n_{rel} \cdot n_{normal} \geq 0$ and 0 when $n_{rel} \cdot n_{normal} < 0$.

## CONTROLLER DESIGN

A total of three controllers for the outer and inner loops of the control system are utilized to achieve precise pointing while maintaining a relatively stable panel configuration when the attitude is converging to a steady state. The passive aerodynamic detumbling control will be employed in the initial phase of the release. As for 3-axis attitude control, the PSM controller will orientates the satellite to the vicinity of the desired attitude, then switch to the square-root PI controller for maintaining the desired orientation. The following sections will introduce each of the controllers used and the conditions under which a specific controller will be chosen.

### *Passive Detumbling Control*

To achieve a stable attitude after the initial release of the satellite with relatively large angular rates in three axes, the passive aerodynamic control is used to damp the angular rates in y and z axes in body frame. In this mode, the four control panels of the satellite will rotate to $\theta = 90^o$ , where $\theta$ is the deflection angle of the control panel, to create the naturally restoring torques that will passively orient the satellite's x-axis in alignment with the velocity vector.

### *Quaternion Feedback Regulator*

The quaternion feedback regulator employs the quaternion error to determine the torques to be exerted on each principal axis has been proven to have asymptotic stability.[18] This controller serves as the outer loop for sensing the attitude error and generating the command input to the inner loop controllers. The three components of command torques determined by the quaternion regulator in body x,y, and z axes can be represented as the control torque vector $u$ through the following equation relating the control output with angular rates and attitude error:

$$u = -\Omega J\omega - D\omega - Kq_e \tag{10}$$

with the first, second, and third terms for handling the nonlinear body rate effect, linear body rate effect, and linear quaternion error, respectively. **D** and **K** are the gain matrices, which can be expressed as $D = dJ$ and $K = kJ$, where d and k are the gains to be tuned. This control algorithm is frequently used for the slow rotation maneuver and can achieve eigenrotation if the gains d and k are tuned according to the method described in[16] for the optimal torque allocation.

### *Panel Selection Method (PSM)*

The backbone of PSM is the PCA first proposed in,[3] and we modified it by relating the selection of configurations with the body angular rates. This is the first inner loop controller that takes the input command from the quaternion regulator and selects the suitable configurations (deflection angles) of control panels for generating the torques as close to the command input as possible.

This discretized proportional controller will select a finite amount of output choices from the prede-

fined output matrix. For each time step in the simulation, PSM will generate a set of possible selections of configurations for each control surface, and the deflection angle for each possible choice is proportional to the modified current angular rates through a constant $gain_\omega$ to be tuned. For each unique angular rate vector, the modified angular rate $\omega_{modified}$ can be written in the equation below:

$$\omega_{modified} = gain_\omega \sqrt{(|\omega_x| + |\omega_y| + |\omega_z|)/3 + constant} \tag{13}$$

where $\omega_x, \omega_y, \omega_z$ denote the angular rates in three principal axes, respectively. The angular rate-based gain is used to better determine the suitable torque according to the current body angular rates and prevent issues such as overshooting when the angular rate is high despite the small attitude error. Once the modified angular velocity is obtained, the possible deflection angle can be found from the following relation with another constant $gain_\theta$:

$$\theta_{max} = gain_\theta \cdot \omega_{modified} \tag{14}$$

where $\omega_{avg}$ represents the averaged angular rates in three body axes, and $\omega_{modified}$ is the quantity denoting the processed angular rate and is served as the input for generating $\theta_{max}$. For each control panel at a given time-step, three possible angles determined from above are created as the potential choices for the output. With four control panels installed, the resulting 3 by 4 choice matrix stores all the possible configuration combinations. Therefore, the choice matrix $\Theta$ will take the form:

$$\Theta = \begin{bmatrix} \theta_{11} & \theta_{21} & \theta_{31} & \theta_{41} \\ \theta_{12} & \theta_{22} & \theta_{32} & \theta_{42} \\ \vdots & \vdots & \vdots & \vdots \\ \theta_{13} & \theta_{23} & \theta_{33} & \theta_{42} \end{bmatrix} \tag{15}$$

where $\theta_{i1} = 0, \theta_{i2} = \theta_{max}, \theta_{i3} = -\theta_{max}, i = 1, 2, 3, 4$ and $j = 1, 2, 3$ are three possible angles to choose from. With a matrix providing 81 possible configurations, the algorithm will then assess which configuration will generate the torque closest to the input command from the quaternion controller. The overall decision-making flowchart can be visualized as in Figure 2. In this figure, $M_a$ is the torque resulting from the aerodynamic force, $M_q$ is the input command torque from the outer loop controllers, $M_{error}$ is the error torque that will be assessed before the algorithm determines the proper final torque output $M_{out}$ to be used to control the satellite.

***Square-Root PI Controller***

The square-root type PI controller is implemented to achieve a stable desired orientation that will take on the inner control loop after the attitude error is small enough. The nonlinear, square-root relation error for the PID controller has been proven to be effective in attenuating the overshoot when the input is too large to drive the system. smoother and faster.[20] Also, if the input signal is too small, the square-root relationship can properly amplify the input, which can't be achieved with the traditional linear input-output relationship. Figure 3. demonstrates the benefit of square root modification:

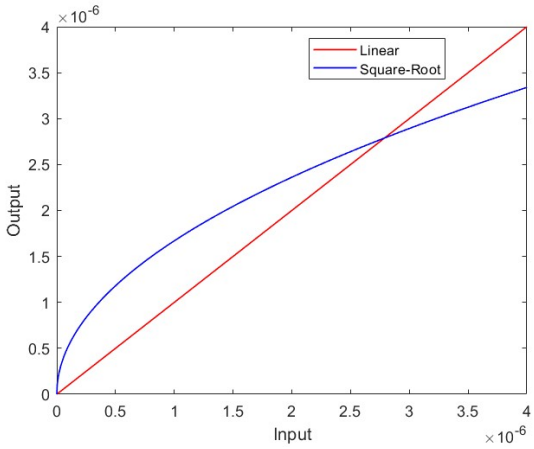


**Figure 3: Comparison of square-root processed input and the traditional linear input**

Applying the square root concept into the PI controller, the equation of control algorithm can be written as:

$$u_{inter,j} = K_{p_j} \sqrt{e_j} + K_{i_j} \int_0^t \sqrt{e_j(\tau)} d\tau, j = 1, 2, 3 \tag{16}$$

where $u_{inter}$ is the intermediate input for the dimension reduction equation to be presented, $K_{p_j}$ represents the proportional gain, $K_{i_j}$ is the gain for the integration term, and $j$ is the free index for three axes.

Due to the error vector of input being only a three-element vector $[e_{M_x}, e_{M_y}, e_{M_z}]$ storing the torque error while there are four control surfaces to be controlled, an additional equation relating the PI controller input and the control surface configuration has been added as :

$$\begin{cases} \theta_1 = -u_{intere,1} + u_{intere,2} \\ \theta_2 = u_{intere,1} + u_{intere,3} \\ \theta_3 = u_{intere,1} + u_{intere,2} \\ \theta_4 = -u_{intere,1} - u_{intere,3} \end{cases} \tag{17}$$

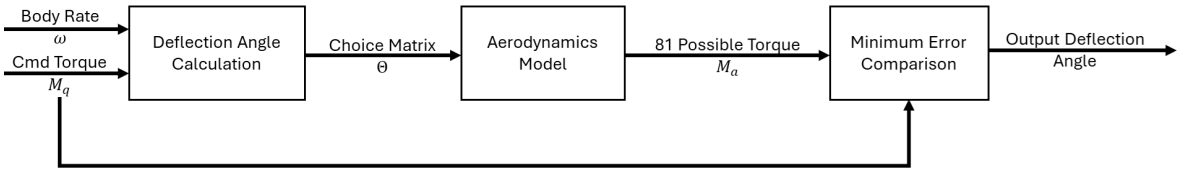


**Figure 2: Decision Making flowchart of PSM controller**

in which $\theta_1 - \theta_4$ represent the deflection angles of each control panel. This equation couples the pitch and yaw control with the roll control to realize the demand of four control surface angle selections with only three inputs from the PI controller.

***Switch Design***

The quaternion error $q_e$ mentioned in Eq.5 is selected as the criteria on when to switch between PSM and PI controllers. The scalar component of $q_e$ is unitary when the attitude error is 0, and this characteristic will then be used to determine attitude error quantitatively. The switch logic of the controllers can be presented as follows:

$$\begin{cases} \text{if } q_e < 0.999, & \text{Using PSM controller} \\ \text{if } q_e \geq 0.999, & \text{Using Square-root PI controller} \end{cases}$$

The overall numerical simulation architecture, including all controllers and models, can be summarized in Figure 4.

## NUMERICAL SIMULATION RESULT AND ANALYSIS

In this section, the focus has been made to four points: the impact of lifetime using the aerodynamics control, the detumbling performance of the active and passive aerodynamic control with a comparison with the conventional B-dot detumbling method using the magnetorquer(MTQ), performance analysis on the real-time attitude tracking maneuvers with two controllers(PSM and square-root PI), and the improvement over the PCA and PSM by the inclusion of switch and square-root PI controller for maintaining a stable flight.

***Simulation Setup***

To demonstrate the feasibility of aerodynamics control and the impact of aerodynamic control surfaces on the lifetime reduction, we propagate the satellite in a simplified orbit with zero eccentricity and inclination, the orbit elements are listed in Table 1. For the circular orbit, with a constant altitude, we can assume the air density is invariant during the propagation for simulations except for lifetime analysis. In the lifetime simulation, the altitude is allowed to vary as the orbit decays in its height. On the other hand, for equatorial orbit, the effect of a rotating atmosphere would be ignored, which reduces the complexity of the simulation. Notably, the orbit element listed in Table 1 will be applied throughout the work. The values for the moment of inertia were based on the CAD data of in-development 3U Cubesat at NCKU.

**Table 1: CubeSat Configs and Kplerian Orbit Elements**

| Items | Values |
|---|---|
| Moment of inertia($kg \cdot m^2$) | Diag[0.0067;0.033;0.034] |
| Eccentricity: | 0 |
| RAAN (deg): | 97 |
| Argument of periapsis (deg): | 0 |
| True anomaly (deg): | 315 |
| Semi-major axis (Km): | 6683.14 |

**Table 2: Simulation Parameters for each Case**

| | |
|---|---|
| **Detumbling Maneuver** | |
| Initial angular rates (rad/sec) | [0.6, -0.5, -0.4] |
| Initial attitude in LVLH (quaternion) | [1; 0; 0; 0] |
| Max magnetic moment for B-dot case ($A \cdot m^2$) | 2 |
| Max simulation tolerance | 0.001 |
| Control panel configuration (deg) | [90; 90; 90; 90] |
| **Real-Time Attitude Tracking Maneuver** | |
| Initial angular rates (rad/sec) | [0, 0, 0] |
| Initial attitude in LVLH (1-2-3 Euler angle) | [0, 0, 0] |
| Desired x-axis attitude (deg) | $6(\sigma(t-50) - \sigma(t-400))$ |
| Desired y-axis attitude (deg) | $4(\sigma(t-400) - \sigma(t-50))$ |
| Desired z-axis attitude (deg) | $5(\sigma(t-50) - \sigma(t-400))$ |
| Max simulation tolerance | 0.0001 |

As for initial condition of simulation setup, a summary is listed in Table 2. The assigned angular rates for the detumbling case are based on the previous simulation setting[20] to cross-validate our work with the reported results. The max magnetic moment of the MTQ is determined by referring to the regular cost-off-shelf MTQ rods used on CubeSat-class satellite. Four control panels are set to $90^o$ in

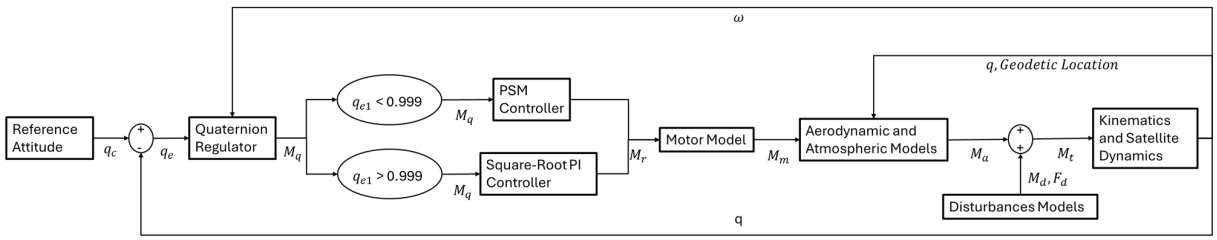


**Figure 4: Simulation Architecture With Controllers and Models**

the passive detumbling case to ensure a maximized stabilizing effect around the straight flight condition. While in the detumbling task with active control, all four panels are allowed to move freely in the range of $-90^o$ to $90^o$.

All initial angular rates are defined to be zeros in the attitude tracking case, and the attitude is expressed in the 1-2-3 convention of Euler angles for easy reading. For generality, a command signal are designed to go back and forth of the zero state, serving a common pointing task in the orbit. The command signal can be expressed in two step function in this work as list in Table 2.

***Lifetime Analysis***

Lifetime is an important measurement of a satellite's mission design, and a significant reduction of lifetime can occur if the control panels aren't properly adjusted to lower the frontal area during nominal operation. A simple simulation of lifetimes for cases where all control panels are in $90^o$ and $0^o$ representing maximum and minimum drag in our satellite configuration, respectively, is conducted to understand the impact of panel configurations on the lifetime. Figure 5 shows the altitudes of perigee and apogee for each case, and the apogee and perigee curves overlap due to the 0 eccentricity in our setting. Significant lifetime reduction happens when the satellite is in the maximum drag configuration that causes the deorbit to occur within 60 days. In the minimum drag configuration where all panels are parallel to the velocity vector, the lifetime is estimated to be 1.5 years, and both values are in good agreement with the previous research efforts.[7]

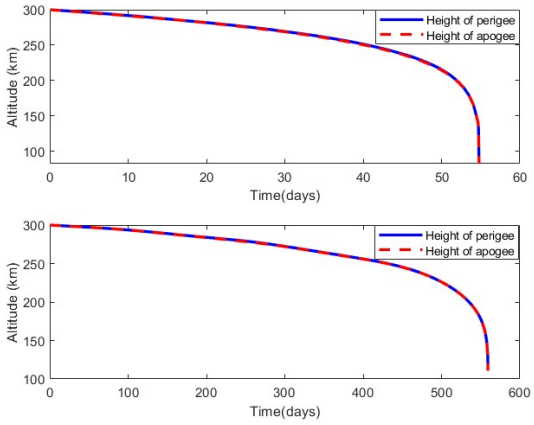


**Figure 5: Time trace of altitude for Cubesat at 300km orbit with maximum(upper one) and minimum (lower one) drag configurations**

***Detumbling Comparison***

Most satellites operating in the LEO environments use the MTQ and the corresponding B-dot algorithm to stable the initial chaotic motion before switching to the reaction wheels for attitude tracking. The MTQ will use the geomagnetic field and the magnetic polar created by MTQ rods to slow down the angular rates in all three body axes. On the VLEO, where the air density is hundreds of times higher than regular LEOs, either active or passive the aerodynamic control methods have the potential to stable the spacecraft in a reasonable period. Therefore, a simulation comparing the performance of both control strategies is performed.

The stability and control properties characterized by the restoring pitching and yawing moments require a naturally stable flying object to maintain the velocity vector aligned with the body x-axis. To have such properties, the control panels should create a negative pitching torque when the pitch angle is positive, and vice versa. The same principle also applies to the yawing motion, and the following Figures 6 and 7 show the effect of attitude with respect to the stabilizing torques, which illustrates that the resulting torques will always push the attitude to the

origin (pitch=yaw=$0^o$).

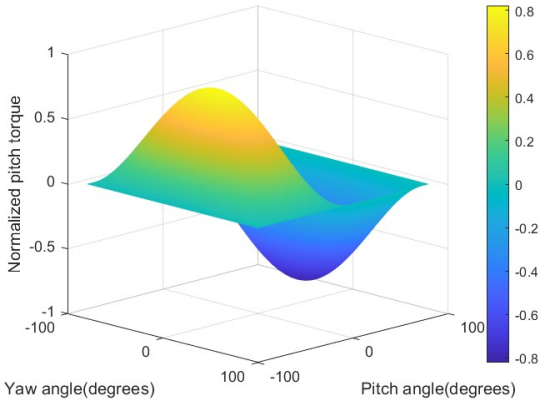


**Figure 6: Stabilizing pitching torque at different pitch and yaw angles**

The symmetricity of plots is the result of zero inclination and eccentricity of orbit such that the pitch angle is equivalent to the angle of attack and yaw angle is the same as sideslip angle in the aviation terms.

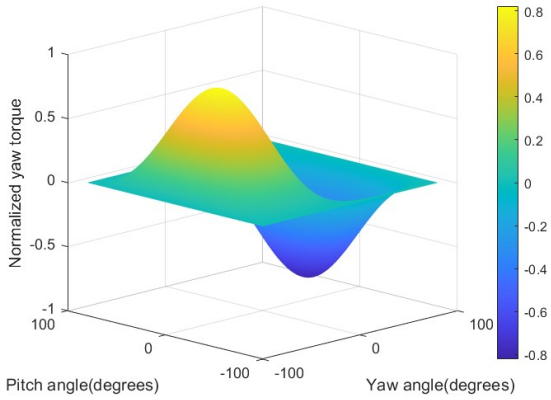


**Figure 7: Stabilizing yawing torque at different pitch and yaw angles**

Figure 8 shows the commonly utilized pitching moment versus pitch angle in analysis the contractility of aircraft to demonstrate the natural stability of the CubeSat. This data is the center slice of the surface plots in previous figures. Because of the symmetricity of our model, the case holds the same for the lateral stability conditions.

Figure 9-11 show the detumbling performances of three cases: MTQ B-dot law method, passive aerodynamic control, and active aerodynamic detumbling to nadir pointing. The conventional B-dot method with MTQ rods can deaccelerate all three angular rates close to zero after an hour as shown in Figure 8, which is a reasonable period for typical CubeSat in the VLEO environments.[20]

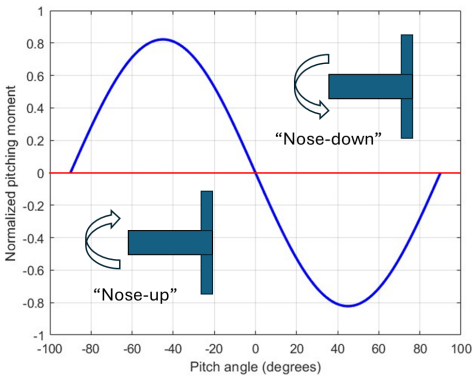


**Figure 8: Stabilizing pitching torque at different pitch angles**

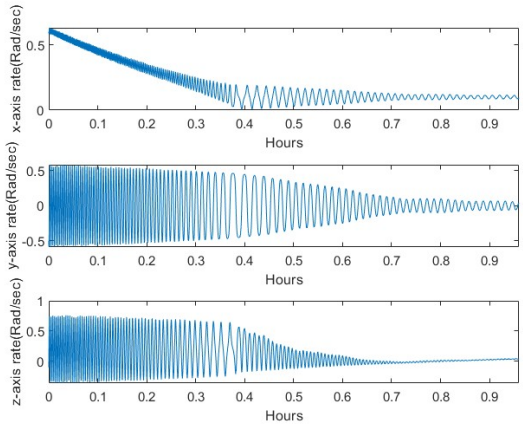


**Figure 9: Body angular rates in three principal axes with B-dot law method**

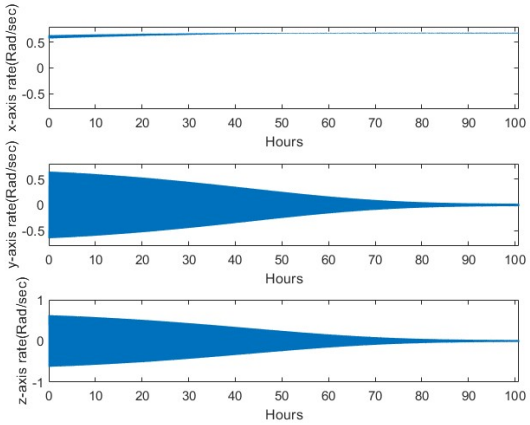


**Figure 10: Body angular rates in three principal axes with passive aerodynamic detumbling**

In Figure 10, the passive aerodynamic detumbling case, when compared with the B-dot method, takes more than 50 times longer to stabilize the spacecraft for the insufficient restoring torques, which is generally not acceptable for most LEO CubeSat design. Moreover, only the pitching and yawing rates can be dampened as described before due to the guaranteed stability only in axes perpendicular to the velocity vector. Despite the mentioned issues, it can still serve as the last resort to maintain a controlled flight in case all controllers aren't working.

To address the issues including long detumbling time and no control over rolling motion associated with the passive control method, active control method is used to stable the satellite as shown in Figure 11. The active aerodynamic controlled detumbling method demonstrates that its performance is comparable to the conventional B-dot method with detumbling times being less than an hour for y and z axes rates, while it will take a longer time to dampen the x-axis angular rates at 2.5 hours. Notably, doesn't like the B-dot method that can only reduce the angular rates to small but finite rates with no attitude tracking capability, the active aerodynamic control not only decrease angular rates in all three axes to zero, but also ensure the a precise nadir pointing orientation can be achieved simultaneously. These traits show that the active aerodynamic control can effectively take on the roles of MTQ and eliminate the need for a second attitude control system for detumbling task.

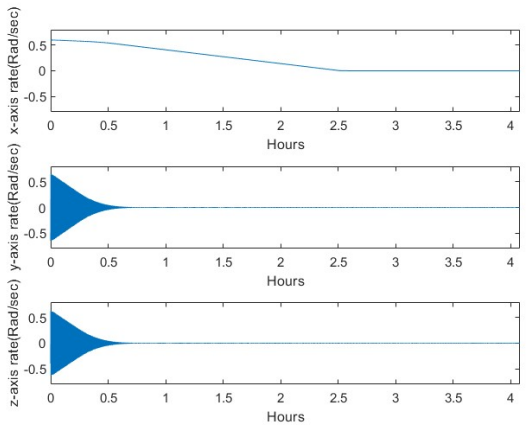


**Figure 11: Body angular rates in three principal axes with active aerodynamic detumbling**

### *3-Axis Real-Time Attitude-Tracking*

This section demonstrates the precise attitude-tracking capability of active aerodynamic control, which is one of the most important functions of any attitude-control system, allowing a satellite to accomplish critical tasks. In most scenarios of attitude-tracking tasks, the desired attitude is a function of time and space. In our simulation, we set up the time-varying steps functions to represent such scenarios with the final attitude going back to the original nadir pointing orientation. By using this setting, it's possible to better illustrate how the control algorithms are switched between PSM and square-root PI, with the goal of proving the stability of response during the switching process. The unique behaviors of each controller can also be concluded at different stages of flight.

To show that the active aerodynamic control can precisely follow the moderate attitude commands, Figure 12 presents the reasonable settling times of responses and the corresponding desired attitude in Euler angles. It will take around 5 min to complete one attitude-varying cycle, which is sufficient for most ground communication or large-area imaging tasks. With the controller modes distinguished by red and blue, we can conclude that the PSM is responsible for the transition phase between different attitudes, while the square-root PI will take over the control once the attitude is stabilized and maintains a constant attitude flight.

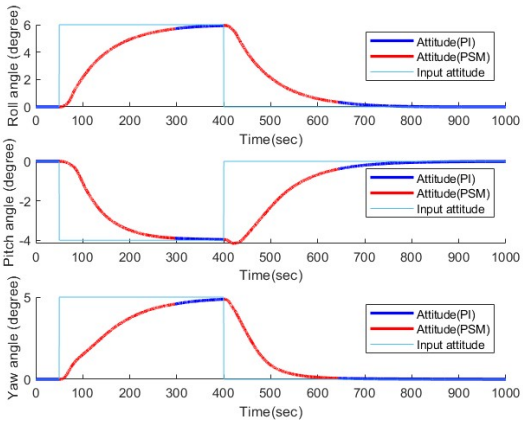


**Figure 12: Time traces of desired and actual attitudes represented in Euler angles**

To clearly illustrate how the controller modes are switched according to the different flights phases, Figure 13 shows that by using the scalar part of quaternion error as a threshold to determine which mode to choose, the controllers can be switched properly to cope with current flight phase with no confusion of mode selection observed.

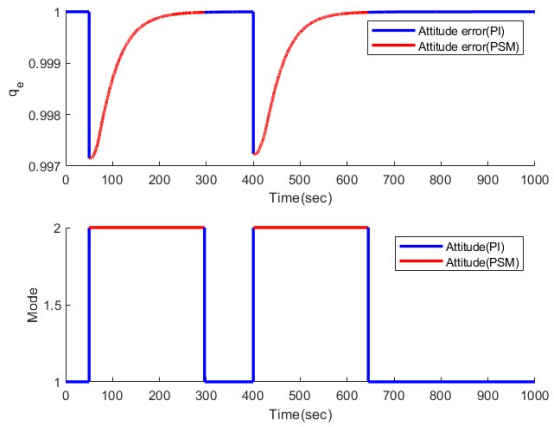


**Figure 13: Time traces of attitude error and the modes being used**

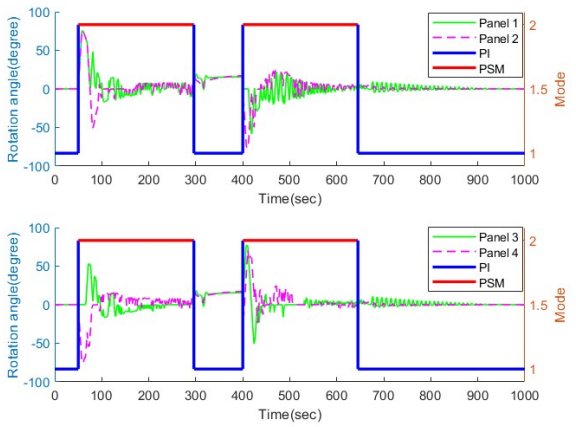


**Figure 14: Time traces of control panel rotational angles and modes used**

Each controller features unique aforementioned behaviors for their responses in terms of attitude and panel rotation. Because both controllers can converge to the desired attitude with little errors, we will investigate their difference through the time trace of the control penal rotation, as shown in Figure 14. Attention should be made to the transition between each mode, and for the first such event occurring at t=50 sec, the mode is switched immediately and the control panels almost saturate for the first few seconds into the transition to provide enough torque. Following that, the panels start to fluctuate and don't reach a stable response before transitioning to the square-root PI controller for stable flight. Upon switching, the response becomes smooth and stable in a short time until 100 sec later, the mode changes again. Around t=650 sec, when the mode is switched back to the PI for stable nadir pointing, there is a prolonged period in which the fluctuations persist several hundred seconds thereafter, and this unstable state will eventually disappear.

Now that square-root PI controller is proven to have a smooth response to minimize the power consumption when the satellite is in stable flight. Figure 15 is focused on the case with only using PSM to emphasize that PSM can't reach a very stable steady state response for it only has a finite 81 combinations of rotation combinations to choose from, and the main distinction can be drawn by observing the period from t=300-400 sec and compare with the Figure 14. For CubeSat with limited battery capacity and a long nadir pointing mission profile, the ever-lasting fluctuation can cause huge unnecessary power waste; therefore, the inclusion of square-root PI controller is important.

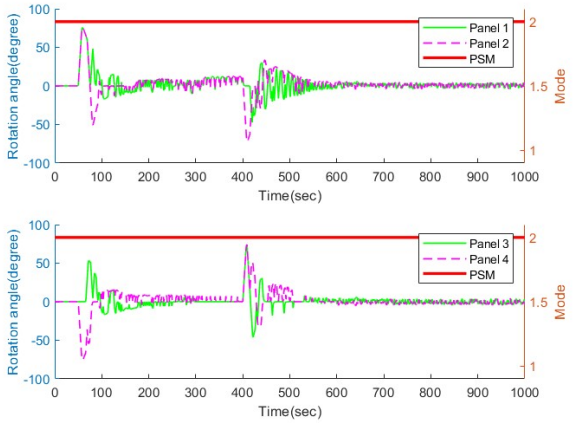


**Figure 15: Time traces of attitude error and the modes being used**

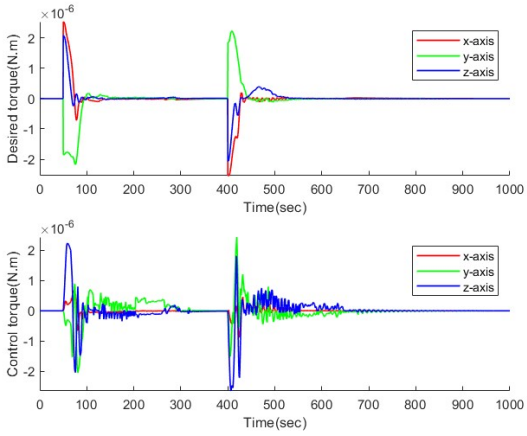


**Figure 16: Time traces of attitude error and the modes being used**

To ensure that the resulting torques are following

the command input, Figure 16 shows the comparison between the command torque from the quaternion error regulator and the actual torque resulted from control panels. The actuating torques for both y and z axes are following nicely with the input torque command, while in the x-axis the resulting rolling torque is much smaller than the command input when both y and z axes torques are relatively large, which can be attributed to the saturation of control panel's rotational limits. And in the active detumbling case where the slow response of the rolling rate is also associated with the saturation, which implies that larger control panels should be fitted to address this issue.

## CONCLUSION

With the simulation results presented, the present work demonstrates the feasibility of using aerodynamic-based control architecture to conduct the precise attitude-pointing task and the responsive detumbling control. Due to the nature of dense air in the VLEO environments, the estimated lifetime is much shorter in comparison with satellite in LEO, and the impact of large drag can be reduced by minimizing the frontal area in nominal operation. Settling times of detumbling for aerodynamic control methods indicate a similar performance to the B-dot method with MTQ rods when correctly actuated. The results also show that even in the worst scenario, when all control panels malfunction, the natural restoring torque can still ensure the two-axes stabilization. For the active attitude pointing, the aerodynamic control system also demonstrates its ability to adjust moderate attitude in an acceptable time.

The newly proposed combined control algorithms, featuring both PSM and square-root PI controllers with the switch, prove to be effective in removing the high-frequency panel fluctuations and enhancing the pointing performance by reducing the attitude error for the steady-state response. Switch design based on the quaternion error as the argument can effectively choose the proper control methods for the fast and smooth attitude response.

This work, in continuation with preceding works, again proves that the deployment of purely aerodynamically actuated satellites in VLEO environments can achieve control tasks traditionally handled by reaction wheels and magnetorquers and therefore reduce the system complexity and weight of the attitude control system. The simulation framework can serve as the foundation for the future development of relevant work and give an overview of the estimated performance of aerodynamic control on 3U cubesat.

Undergoing future works, including the data-driven-based control algorithms to handle the uncertainties associated with the changing atmospheric conditions at different altitudes and even on other planets like Mars. Other proposed developments will discover the possibility of using pure aerodynamic control to conduct the formation flight that is usually realized through a minimized thrusters on suitable for CubeSat application.

## ACKNOWLEDGEMENT

I am grateful to Professor Mehran Mesbahi, at the University of Washington, for his advice and to my friends at National Cheng Kung University and at the University of Washington for their contributions to this paper.

## References

[1] Vittorio Bombelli, Dieter Simon, Jean-Luc Morel, and Ton Marée. Economic benefits of the use of non-toxic mono-propellants for spacecraft applications. In *39th AIAA/ASME/SAE/ASEE Joint Propulsion Conference and Exhibit*, Joint Propulsion Conferences. American Institute of Aeronautics and Astronautics.

[2] N.H. Crisp, P.C.E. Roberts, F. Romano, K.L. Smith, V.T.A. Oiko, V. Sulliotti-Linner, V. Hanessian, G.H. Herdrich, D. García-Almiñana, D. Kataria, and S. Seminari. System modeling of very low earth orbit satellites for earth observation. *Acta Astronautica*, pages 475–491, 2021.

[3] Sabrina Livadiotti, Nicholas H. Crisp, Peter C. E. Roberts, Vitor T. A. Oiko, Simon Christensen, Rosa Maria Domínguez, and Georg H. Herdrich. Uncertainties and design of active aerodynamic attitude control in very low earth orbit. *Journal of Guidance, Control, and Dynamics*, 45:859–874, 2022.

[4] Christoph Steiger, Massimo Romanazzo, Pier Paolo Emanuelli, Rune Floberghagen, and Michael Fehringer. The deorbiting of esa's gravity mission goce - spacecraft operations in extreme drag conditions. 2014.

[5] Anthony Shao Christianna Taylor Richard Van Allen James Wertz, Nicola Sarzi-Amade. Moderately elliptical very low orbits (mevlos) as a long-term solution to orbital debris. 2012.

[6] J. Virgili Llop, P.C.E. Roberts, Zhou Hao, L. Ramio Tomas, and V. Beauplet. Very low earth orbit mission concepts for earth observation: Benefits and challenges. 2014. Reinventing Space Conference ; Conference date: 18-11-2014 Through 20-11-2014.

[7] Valentín Cañas, D González, Jonathan Becedas, Rosa Dominguez, Peter Roberts, Nicholas Crisp, Vitor Oiko, S Edmondson, Stephen Worrall, Sarah Haigh, Katharine Smith, Rachel Lyons, Sabrina Livadiotti, C Huyton, Luciana Sinpetru, Silvia Donaire, Daniel García-Almiñana, M Nieto, C Muñoz, and B. Heisserer. Attitude control for satellites flying in vleo using aerodynamic surfaces. *Journal of the British Interplanetary Society*, pages 103–112, 2020.

[8] J. Auret and Willem Steyn. Design of an aerodynamic attitude control system for a cubesat. *62nd International Astronautical Congress 2011, IAC 2011*, pages 9009–9017, 2011.

[9] Michael Gargasz. Optimal spacecraft attitude control using aerodynamic torques. page 91, 2007.

[10] R. RAVINDRAN and P. C. HUGHES. Optimal aerodynamic attitude stabilization of near-earth satellites. *Journal of Spacecraft and Rockets*, pages 499–506, 1972.

[11] David Mostaza Prieto, Benjamin P. Graziano, and Peter C.E. Roberts. Spacecraft drag modelling. *Progress in Aerospace Sciences*, pages 56–65, 2014.

[12] Jose F. Padilla and Iain D. Boyd. Assessment of gas-surface interaction models for computation of rarefied hypersonic flow. *Journal of Thermophysics and Heat Transfer*, pages 96–105, 2009.

[13] Dean C. Wadsworth, Douglas B. VanGilder, and Virendra K. Dogra. Gas-Surface Interaction Model Evaluation for DSMC Applications. *AIP Conference Proceedings*, pages 965–972, 05 2003.

[14] B. Wie, H. Weiss, and A. Arapostathis. Quarternion feedback regulator for spacecraft eigenaxis rotations. *Journal of Guidance, Control, and Dynamics*, pages 375–380, 1989.

[15] Zhipeng Duan and Hao Ma. Chapter four - pressure drop and heat transfer in the entrance region of microchannels. volume 52 of *Advances in Heat Transfer*, pages 249–333. Elsevier, 2020.

[16] J. M. Picone, A. E. Hedin, D. P. Drob, and A. C. Aikin. Nrlmsise-00 empirical model of the atmosphere: Statistical comparisons and scientific issues. *Journal of Geophysical Research: Space Physics*, pages SIA 15–1–SIA 15–16, 2002.

[17] D.A. Vallado and W.D. McClain. *Fundamentals of Astrodynamics and Applications*. Fundamentals of Astrodynamics and Applications. Microcosm Press, 2001.

[18] W.E. Wiesel. *Spaceflight Dynamics*. Advances in the astronautical sciences. McGraw-Hill, 1997.

[19] Fernando Reyes, Jaime Cid, Miguel Angel Limon, and Manuel Cervantes. Square root - type control for robot manipulators. *International Journal of Advanced Robotic Systems*, page 39, 01 2013.

[20] Rishav Sharma, Rohit Kawari, Sagar Bhandari, Shishir Panta, Rakesh Prajapati, and Nanda Adhikari. *Simulation of CubeSat Detumbling Using B-Dot Controller*, pages 541–553. 03 2021.